

1 Muon content in air showers between 10 PeV and 1 2 EeV determined from measurements with 3 KASCADE-Grande

J.C. Arteaga-Velázquez^{*1}, D. Rivera-Rangel¹, W.D. Apel², K. Bekk², M. Bertaina³, J. Blümer^{2,4†}, H. Bozdog², E. Cantoni^{3,6}, A. Chiavassa³, F. Cossavella⁴, K. Daumiller², V. de Souza⁷, F. Di Pierro³, P. Doll², R. Engel^{2,4}, D. Fuhrmann⁸, A. Gherghel-Lascu⁵, H.J. Gils², R. Glasstetter⁸, C. Grupen⁹, A. Haungs², D. Heck², J.R. Hörandel¹⁰, T. Huege², K.-H. Kampert⁸, D. Kang⁴, H.O. Klages², K. Link⁴, P. Łuczak¹¹, H.J. Mathes², H.J. Mayer², J. Milke², C. Morello⁶, J. Oehlschläger², S. Ostapchenko¹², T. Pierog², H. Rebel², M. Roth², H. Schieler², S. Schoo², F.G. Schröder², O. Sima¹³, G. Toma⁵, G.C. Trinchero⁶, H. Ulrich², A. Weindl², J. Wochele², J. Zabierowski¹¹ - KASCADE-Grande Collaboration[‡]

¹ Instituto de Física y Matemáticas, Universidad Michoacana, Morelia, Mexico

² Institut für Kernphysik, KIT - Karlsruhe Institute of Technology, Germany

³ Dipartimento di Fisica, Università degli Studi di Torino, Italy

⁴ Institut für Experimentelle Teilchenphysik, KIT - Karlsruhe Institute of Technology, Germany

⁵ Horia Hulubei National Institute of Physics and Nuclear Engineering, Bucharest, Romania

⁶ Osservatorio Astrofisico di Torino, INAF Torino, Italy

⁷ Universidade São Paulo, Instituto de Física de São Carlos, Brasil

⁸ Fachbereich Physik, Universität Wuppertal, Germany

⁹ Department of Physics, Siegen University, Germany

¹⁰ Dept. of Astrophysics, Radboud University Nijmegen, The Netherlands

¹¹ National Centre for Nuclear Research, Department of Astrophysics, Lodz, Poland

¹² Frankfurt Institute for Advanced Studies (FIAS), Frankfurt am Main, Germany

¹³ Department of Physics, University of Bucharest, Bucharest, Romania

E-mail: arteaga@ifm.umich.mx

Muons in extensive air showers (EAS) are a sensitive probe for the primary cosmic ray mass and the physics of hadronic interactions at very high energies, hence it is important to precisely measure and carefully analyze this particular shower component. In practice, however, such measurements are difficult to carry out due to the penetrating nature of muons and their low density in the shower. This way just in a few experimental facilities the shower muon component has been measured event-by-event in combination with other EAS observables. One of them was the multicomponent air shower experiment KASCADE-Grande, which was designed to study cosmic rays in the energy interval from 1 PeV to 1 EeV and was located at the site of the Karlsruhe Institute of Technology, Germany at 110 m a.s.l. In this work, we will present an analysis of the KASCADE-Grande data in terms of the muon content ($E_\mu > 230$ MeV) of cosmic-ray induced air showers as a function of the primary energy ($E = 10$ PeV – 1 EeV) and the zenith angle ($< 35^\circ$). We test also the predictions on the shower muon content of the post-LHC hadronic interaction models EPOS-LHC, QGSJET-II-04, SIBYLL 2.3 and SIBYLL 2.3c by comparing the model expectations with experimental results.

36th International Cosmic Ray Conference -ICRC2019-
July 24th - August 1st, 2019
Madison, WI, U.S.A.

4 1. Introduction

5 At high-energies, cosmic ray collisions with the Earth's upper atmosphere produce an ex-
6 tensive air shower (EAS) of particles (γ 's, e^\pm 's, muons, hadrons, etc.), whose study can give us
7 information about the characteristics of the primary radiation and the physics of hadronic interac-
8 tions at energies and phase space regions not accessible yet to man-made accelerators. Among the
9 air shower observables that are measured to get access to the composition of cosmic rays and the
10 hadronic processes that occurs in the cascade of particles, we find the muon content.

11 In this work, the total muon number in cosmic-ray induced EAS was investigated with the
12 KASCADE-Grande experiment. Measurements were performed as a function of the primary en-
13 ergy in the range $E = 10^{16}$ eV $- 10^{18}$ eV, for three different zenith angle intervals: $[0^\circ, 19.34^\circ)$,
14 $[19.34^\circ, 27.93^\circ)$ and $[27.93^\circ, 35^\circ]$. The results will be presented in this paper in comparison with
15 the predictions of four post-LHC hadronic interaction models. A discussion will be also shown,
16 where it will be seen the implications of the muon data for the composition of cosmic rays and the
17 performance of the hadronic interaction models.

18 2. The KASCADE-Grande experiment, measured data and MC simulations

19 KASCADE-Grande was a ground-based air-shower observatory dedicated to investigate the
20 energy spectrum, composition and arrival direction of cosmic rays in the energy range from 10^{15}
21 to 10^{18} eV [1]. The experiment was located at the Karlsruhe Institute of Technology (110 m a.s.l.,
22 1022 g/cm^2 atmospheric depth) in Karlsruhe, Germany, and consisted of several particle detector
23 systems aimed to measure with high precision different components and properties of the EAS.
24 One of the main detector systems of the experiment was the Grande array (0.5 km^2 of area). It
25 was composed of 37 scintillator detectors and was employed to estimate the shower core position
26 at ground, the angle of incidence and the shower size or total number of charged particles of the
27 event, N_{ch} , i.e. e^\pm 's plus μ 's ($E_{ch} > 3 \text{ MeV}$ for vertical incidence). Another important detector
28 system was the set of 192 shielded scintillator detectors from the KASCADE array ($200 \times 200 \text{ m}^2$)
29 [2], which provided information about the total number of muons, N_μ , with $E_\mu > 230 \text{ MeV}$ in the
30 shower. More details about the experiment and the reconstruction procedures can be found in [1].

31 The present study was carried out with data collected during the full data acquisition period
32 of the experiment, i.e., from December 2003 up to November 2012. In order to diminish the effect
33 of systematic uncertainties in the results, several selection cuts were applied to the data. For the
34 analysis, events measured during stable data acquisition runs with no hardware problems were
35 considered. In addition, data that passed successfully the full reconstruction chain were included
36 [1]. Besides, EAS cores were required to be located within the limits of a central area of $2.25 \times$
37 10^5 m^2 of the experiment and within radial distances $R = [150 \text{ m}, 650 \text{ m}]$ measured from the center
38 of the KASCADE array (see fig. 1, left). Besides, events with $\theta \geq 35^\circ$ were rejected. Finally, low
39 energy events with $N_\mu \leq 3 \times 10^4$ and $N_{ch} \leq 1.1 \times 10^4$, and activated less than 11 Grande stations
40 were removed. With the above selection cuts, we got 1.13×10^7 experimental events.

41 For this study, MC simulations were generated. The production and development of the EAS
42 were simulated without thinning with CORSIKA v7.5 [3] and the passage of the shower particles

*Speaker.

†Head of KIT Division V - Physics and Mathematics

‡for collaboration list see PoS(ICRC2019)1177

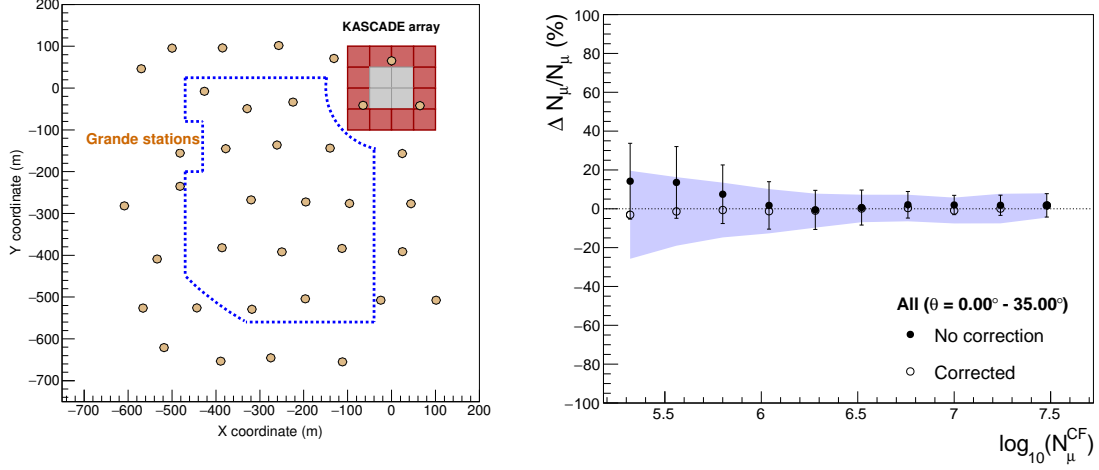


Figure 1: Left: Layout of the KASCADE-Grande experiment. Small circles represent the Grande stations. The KASCADE array is seen at the upper right hand of the figure. KASCADE detectors are arranged in 16 clusters (big squares). The outer 12 clusters (red squares) contain the 192 shielded plastic scintillator stations used for muon measurements. The dotted region shows the effective area selected for the present analysis. **Right:** The relative bias on the reconstructed (corrected) muon number as a function of the reconstructed (corrected) muon number for SIBYLL 2.3c. The full circles represent the bias before applying the correction for systematic errors, and the open circles, the bias of the corrected muon number. The error bars (band) are (is) the 1σ statistical errors of the relative systematic uncertainties for the reconstructed (corrected) muon size.

43 through the detectors, with GEANT 3.21 [4]. At low energies ($E_h \leq 200$ GeV), hadronic interactions of the EAS were simulated with Fluka 2011.2 [5], while at higher energies, QGSJET-II-04
 44 [6], EPOS-LHC[7], SIBYLL 2.3 [8] and SIBYLL 2.3c [9] were employed. In each case, MC
 45 events were generated for $\theta < 42^\circ$ and $E = [10^{14} \text{ eV}, 3 \times 10^{18} \text{ eV}]$ using an E^γ primary spectrum
 46 with spectral index $\gamma = -2$. For the analysis, the MC events were weighted in order to simulate
 47 a power-law spectrum with $\gamma = -2.8, -3.0$ and -3.2 . MC data samples were produced for five
 48 primary nuclei: H, He, C, Si and Fe, each of them with roughly the same number of events. Besides
 49 two additional samples were generated, one called the mixed data set with all primary elements on
 50 equal abundances, and another one called the GSF data sample, where individual cosmic ray abun-
 51 dances and spectra were modeled after the Global Spline Fit model described in [10]. The latter
 52 was obtained from fits to cosmic ray data of different experiments as KASCADE-Grande. All MC
 53 data sets were processed with the same reconstruction algorithm employed with the experimental
 54 events [1]. For the analysis we also applied the same quality cuts for both MC and measured data.
 55

56 According to MC simulations the maximum efficiency for the selected data is reached at
 57 $\log_{10}(E/\text{GeV}) = 7.1 \pm 0.2$ depending of the primary nuclei and the arrival direction of the EAS.
 58 On the other hand, the mean shower core and angular biases are ≤ 10 m and $\leq 0.6^\circ$, respectively,
 59 while the bias ($\Delta N_\mu = N_\mu - N_\mu^{True}$) in the muon size is smaller than 20% (see, for example, fig. 1,
 60 right). In addition, by comparing experimentally measurements performed independently with the
 61 KASCADE and the Grande arrays, it was found out that the systematic uncertainty in the shower
 62 size is $< 15\%$.

63 Finally, we have improved the accuracy of N_μ , for both MC and measured data, by correcting

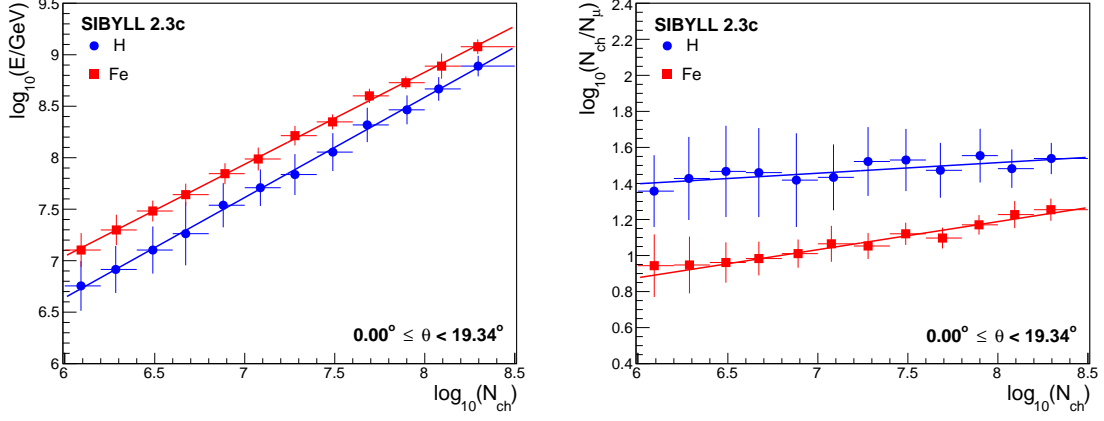


Figure 2: **Left:** The mean logarithmic energy as a function of the logarithm of the shower size predicted by SIBYLL 2.3c for iron nuclei (red squares) and protons (blue circles). The respective fits with eq. (2.1) are shown with red and blue lines, respectively. **Right:** The mean logarithm of the N_{ch}/N_{μ} ratio against the logarithm of the shower size expected from SIBYLL 2.3c for iron nuclei (red squares) and protons (blue circles). The results of the fits a power law formula are shown with red and blue lines, correspondingly. The left and right panels were done for vertical data with zenith angles less than 19.34° .

64 the reconstructed muon number for systematic biases using a correction function defined as in
 65 [11]. The correction function is a parameterization of the systematic uncertainties of N_{μ} in terms
 66 of the arrival direction, the muon content and the core position of the EAS. It was estimated from
 67 MC simulations for each post-LHC model using the mixed data set for an E^{-3} primary spectrum.
 68 The muon correction function was applied to both the MC simulations and the measured data.
 69 MC simulations and correction functions from different post-LHC models were not mixed. In the
 70 same way, only KASCADE-Grande data and MC simulations treated with the same correction
 71 function were compared in the following analysis. After correcting the muon data for systematic
 72 uncertainties, the final bias on N_{μ} becomes smaller than 8% (e.g. fig. 1, right).

73 In order to calibrate the primary energy of each event, the procedure described in [11] was
 74 followed. First, data are divided in different θ intervals and then in each of them, energy is assigned
 75 with a power-law formula calibrated with MC simulations,

$$\log_{10}(E/\text{GeV}) = [a_H + (a_{Fe} - a_H) \cdot k] \cdot \log_{10} N_{ch} + [b_H + (b_{Fe} - b_H) \cdot k], \quad (2.1)$$

76 where k depends on the N_{ch}/N_{μ} ratio. It takes the value 0 for protons and 1 for iron nuclei. In
 77 eq. (2.1), the coefficients a , b are obtained from fits to model predictions (see, for example, fig. 2,
 78 left). For this study, data was separated according to the following zenith angle bins: $[0^{\circ}, 19.34^{\circ}]$,
 79 $[19.34^{\circ}, 27.93^{\circ}]$ and $[27.93^{\circ}, 35^{\circ}]$.

80 3. Results and discussions

81 The mean of the logarithm of the total muon number of EAS measured with KASCADE-
 82 Grande as a function of the logarithm of the estimated primary energy is shown in fig. 3 for our three
 83 zenith angle intervals. The data are compared with predictions of the four post-LHC models for
 84 iron nuclei and protons, which are shown with bands. The mean values of the data were estimated

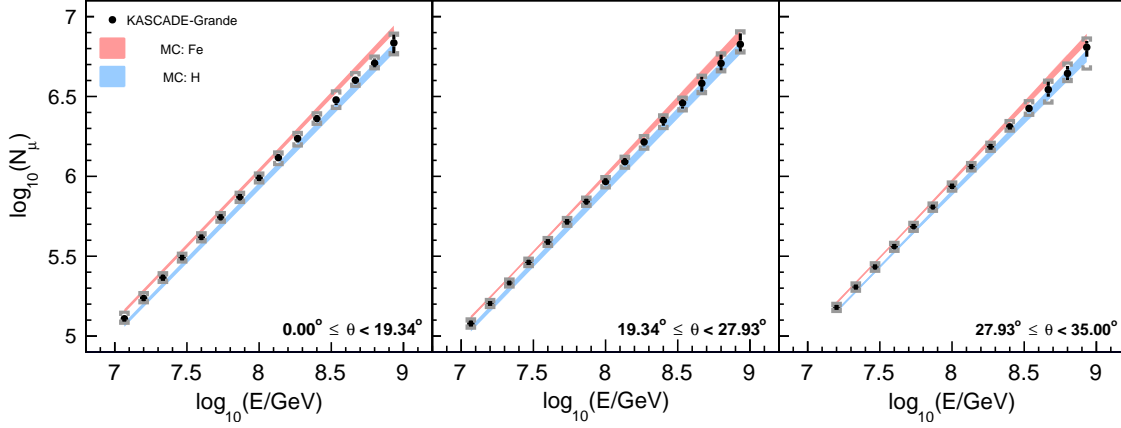


Figure 3: The mean total muon content of EAS as a function of the estimated primary energy as estimated from measurements with the KASCADE-Grande experiment (data points). The total systematic errors are shown with square brackets and the statistical errors (errors on the mean) with error bars. The data are compared with the predictions of the post-LHC models: QGSJET-II-04, EPOS-LHC, SIBYLL 2.3 and SIBYLL 2.3c, for hydrogen and iron nuclei, which are shown with the lower blue and an upper red bands, respectively. The bands covers the range of variations of the MC expectations. Data is presented for three different zenith angle intervals.

85 as an average of the different values obtained after correction and calibration of the experimental
 86 measurements with the different post-LHC hadronic interaction models. Statistical and systematic
 87 uncertainties were also estimated and are displayed in the above figure. The systematic errors
 88 include different uncertainty sources added in quadrature, in particular, the uncertainties in the
 89 muon correction function and the muon lateral distribution function, the biases of the corrected
 90 N_μ , the shower size and the estimated energy and uncertainties on the primary spectral index. It is
 91 seen from the plot 3 that the muon data above 230 MeV at sea level measured with KASCADE-
 92 Grande in the primary energy range 10^{16} eV to 10^{18} eV lies between the model predictions for
 93 protons and iron nuclei.

94 In fig. 4, the muon number has been divided by the primary energy in order to appreciate the
 95 details of the evolution of N_μ with E . The data have been compared with the H and Fe predictions
 96 of the post-LHC models in different panels. In each of them, the model used for the comparison
 97 and to correct/calibrate the MC/measured data is shown. For reference, the expectations from the
 98 GSF composition model were also added in the plot. From the graphs on fig. 4, it is observed that
 99 the measured N_μ does not follow a power-law behaviour with the energy as expected from MC
 100 simulations for pure composition. That seems to be a consequence of an evolution in the relative
 101 abundances of cosmic ray nuclei in the data, behavior which is also seen in the predictions from
 102 the GSF composition model. Differences in the inferred composition from the KASCADE-Grande
 103 data using the distinct post-LHC models are also observed. The lightest composition was obtained
 104 when using EPOS-LHC, and the heaviest, when employing SIBYLL 2.3c. Those differences seem
 105 to be due to distinct predictions in the muon content of EAS: more muons for EPOS-LHC and fewer
 106 for SIBYLL 2.3c in comparison with the other post-LHC models [12]. Even more, differences in
 107 composition within the framework of the same hadronic interaction models are also appreciated for
 108 different zenith angle bins.

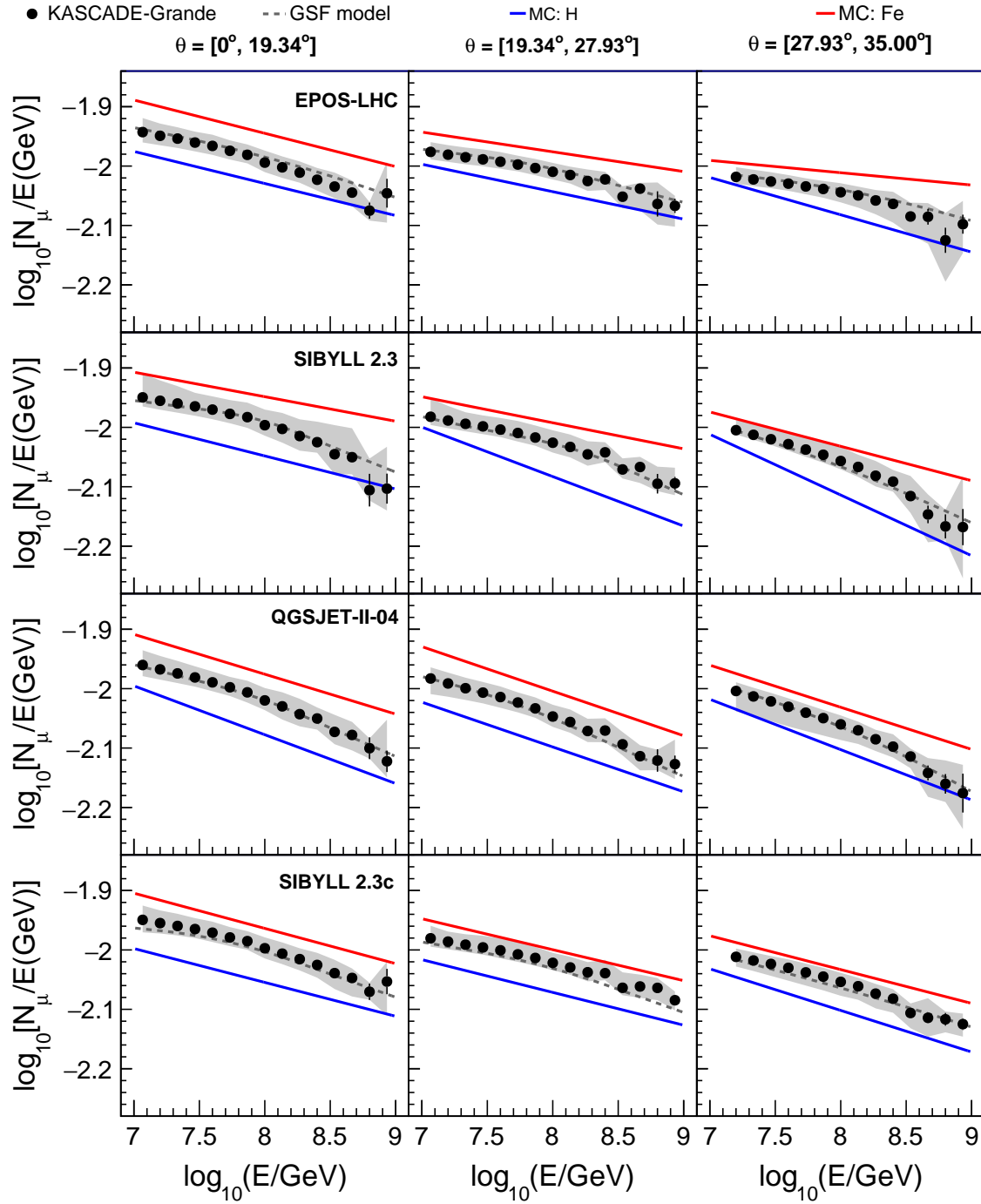


Figure 4: Measured (solid circles) and predicted (lines) mean values of the logarithm of the ratio $N_\mu/E(\text{GeV})$ as a function of the estimated primary energy for different post-LHC hadronic interaction models and three zenith angle ranges. The red upper lines represent the expectations for iron nuclei, and the lower blue lines, for protons. The dashed lines are the predictions from the GSF composition model. The total systematic errors of the data are given by the gray band, and the statistical errors on the mean, by the error bars.

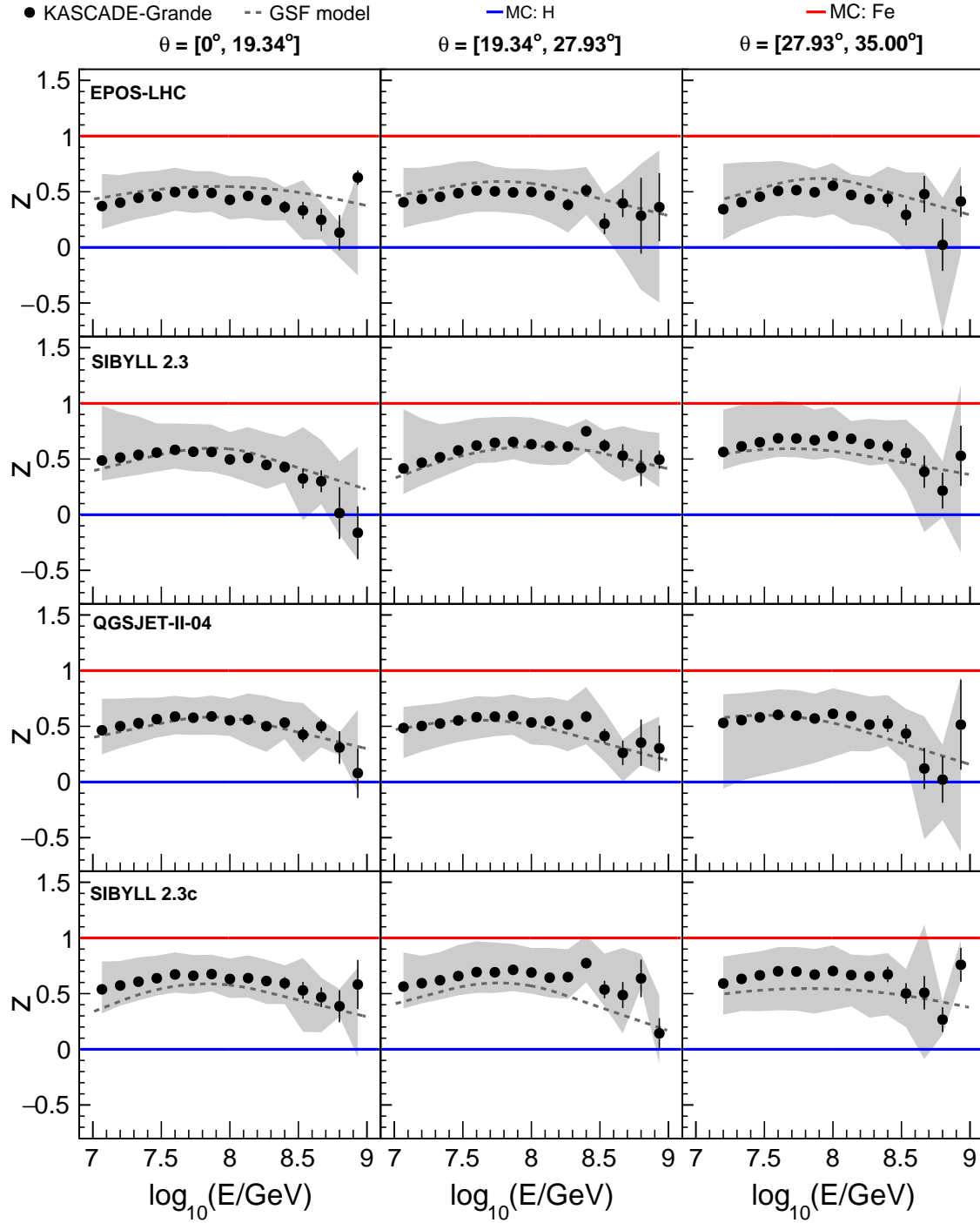


Figure 5: Measured (solid circles) and predicted (lines) mean values of $z = [\ln(N_\mu^{exp}) - \ln(N_\mu^H)] / [\ln(N_\mu^{Fe}) - \ln(N_\mu^H)]$ as a function of the estimated primary energy for different post-LHC hadronic interaction models and three zenith angle ranges. The red upper lines represent the expectations for iron nuclei ($z = 1$), and the lower blue lines, for protons ($z = 0$). The dashed lines are the predictions from the GSF composition model. The total systematic errors of the data are given by the gray band, and the statistical errors on the mean, by the error bars.

109 To study in more detail the dependence of N_μ with the primary energy, the z -value, as defined
 110 in [14] (i.e., $z = [\ln(N_\mu^{exp}) - \ln(N_\mu^H)] / [\ln(N_\mu^{Fe}) - \ln(N_\mu^H)]$) was estimated. Here, N_μ^{exp} is the exper-
 111 imental value, and $N_\mu^{H,Fe}$, the expectations from the model. The mean values of this quantity are
 112 plotted in fig. 5 against the estimated EAS energy and different θ intervals using the measured
 113 data and the models QGSJET-II-04, EPOS-LHC, SIBYLL 2.3 and SIBYLL 2.3c. The results are
 114 compared with the predictions for pure iron and hydrogen nuclei, for which $z = 1$ and 0 , respec-
 115 tively. In this figure, it is observed that the inferred cosmic ray composition is slightly heavier for
 116 high zenith angles and high energies, which implies a problem within the models to describe N_μ at
 117 different θ and E values. These plots seem to support previous results from KASCADE-Grande,
 118 which show that several high-energy hadronic interaction models are not able to describe the zenith
 119 angle evolution of the shower muon content of EAS [13]. Finally, in fig. 5, the same tendency in
 120 the energy evolution of z is observed independently of the post-LHC model: z grows up to $\sim 10^{17}$
 121 eV, and then it seems to decrease, which implies an evolution towards a heavier composition from
 122 10 PeV to 100 PeV and towards a lighter one above 100 PeV. The latter seems to be in agreement
 123 with the light/heavy composition studies of cosmic rays performed with KASCADE-Grande [15].
 124 The same tendency is observed in the GSF model.

125 4. Conclusions

126 KASCADE-Grande muon data above 230 MeV at sea level in the primary energy range from
 127 10 PeV to 1 EeV were compared with predictions of the QGSJET-II-04, EPOS-LHC, SIBYLL 2.3
 128 and SIBYLL 2.3c hadronic interaction models. It was found that the measured muon number lies
 129 between model predictions for hydrogen and iron nuclei and it was also observed that the inferred
 130 cosmic ray composition from the muon data shows a dependence with the model, zenith angle and
 131 energy (slightly heavier for inclined EAS and high energy showers). The results seem to support
 132 previous findings of KASCADE-Grande about a problem in the predicted evolution of N_μ with the
 133 zenith angle.

134
 135 **Acknowledgements:** One of the authors wants to thank the partial support from CONACYT
 136 and the Consejo de la Investigación Científica de la Universidad Michoacana.

137 References

- 138 [1] W.D. Apel et al., *NIM A* **620** 202 (2010).
 139 [2] T. Antoni et al., *NIM A* **513** (2003) 490.
 140 [3] D. Heck et al., Report No. FZKA 6019, Forschungszentrum Karlsruhe-Wissenschaft Berichte (1998).
 141 [4] R. Brun, F. Carminati, *CERN Program Library Long Writeup W5013* (1993).
 142 [5] A.Fasso et al., Report CERN-2005-10, INFN/TC-05/11, SLAC-R-773 (2005).
 143 [6] S. Ostapchenko, *Phys. Rev. D* **83** (2011) 014018.
 144 [7] T. Pierog et al., *Phys. Rev. C* **92**, (2015) 034906.
 145 [8] F. Riehn et al., Proc. of the *34th ICRC*, PoS (ICRC2015) **558**.
 146 [9] F. Riehn et al., Proc. of the *34th ICRC*, PoS (ICRC2017) **301**.
 147 [10] H. P. Dembinski et al., PoS (ICRC2017) **533**.
 148 [11] W.D. Apel et al., *Astrop. Phys.* **36** 183 (2012).
 149 [12] D. Kang et al., these proceedings.
 150 [13] W.D. Apel et al., *Astrop. Phys.* **95** 25 (2017); J. C. Arteaga-Velazquez et al., EPJ Web of Conferences 172, (2018)
 151 07003.
 152 [14] H.P. Dembinski et al., arxiv 1902.08124v1 [astro-ph].
 153 [15] W.D. Apel et al., *PRD* **87** (2013) 081101; W.D. Apel et al., *PRL* **107** (2011) 171104.